Studying Static, Dynamic and Transport Properties of Mg_3Bi_2

F. Kayadibi[a,*], S.D. Günay[b] and Ç. Taşseven[b]

[a]Department of Physics, Science and Art Faculty, Kocaeli University, Umuttepe Campus, 41380, Kocaeli, Turkey

[b]Department of Physics, Faculty of Science, Yildiz Technical University, Davutpaşa Campus, 34210, Istanbul, Turkey

(Received January 19, 2015)

In this study, new potential parameters for Mg_3Bi_2 are proposed which is the Born–Mayer–Huggins type potential. Static, dynamic and transport properties are studied for this material from 300 K up to 1600 K with classical molecular dynamics simulation. Mechanical properties; like elastic constants (C_{11}, C_{12}, C_{13}, C_{33}, C_{44}), bulk modulus and shear modulus are found. All these data are compared with the limited number of experimental and first-principle studies. Our results give a good description of the Mg_3Bi_2 system: lattice constants, $\alpha \rightarrow \beta$ transition temperature, melting temperature, diffusion coefficient, density and mechanical properties are promising.

DOI: 10.12693/APhysPolA.128.440

PACS: 83.10.Rs, 34.20.Gj, 66.30.H–, 66.30.Fq, 62.20.–x, 65.40.–b

1. Introduction

Scientists have investigated the alloys with magnesium in recent years for its technological applications in automobile and aerospace industry because of its low density and high strength [1, 2]. Mg_3Bi_2 has been used in technology at various fields, such as Li-ion batteries [3], thermoelectric element [4] and photoconduction [5]. Some groups have been focused on this material; the optical and semiconducting nature of Mg_3Bi_2 had been investigated by Watson et al. [6]. Bi ion concentration in magnesium alloys had been studied and their effect on heat resistance had been explained by Yuan et al. [7, 8]. Solid Mg_3Bi_2 is a metal and the liquid Mg_3Bi_2 is a semiconductor so that material has a metal–nonmetal transition [9]. These studies have made it more interesting to work on Mg_3Bi_2 molecule.

The structure of α-Mg_3Bi_2 is a hexagonal anti-La_2O_3 type structure with the space group of $P3m1$ [10]. The α phase of Mg_3Bi_2 exists at room temperature up to 976 K and β phase exists in the range 976–1094 K. Mg_3Bi_2 is a superionic conductor in β phase that Barnes et al. [11] and Howells et al. [12] had done neutron diffraction experiments on β-Mg_3Bi_2 and concluded that they had observed mobile Mg^{2+} ions with Bi^{3-} ions forming the rigid lattice. The electronic and structural properties of liquid $Mg--Bi$ alloy are investigated by Guo et al. [13]. First principles molecular dynamics simulation of liquid Mg_3Bi_2 has also been calculated by Wijs [9] and Hao et al. [14]. Structural and elastic properties of solid Mg_3Bi_2 is calculated by Zhou et al. [15] and Sedighi et al. [16] by first-principles calculations.

Despite these studies, there are a limited number of studies on Mg_3Bi_2 and for this reason only some parts of the physical properties exist. To our knowledge, static, dynamic, mechanical and transport properties below the melting point are insufficient in the literature for both with simulation and experimental study. In this study, we have performed classical molecular dynamics simulations mainly to investigate these properties such as lattice constants, radial distribution functions, mean square displacements, diffusion coefficient, heat capacity, bulk modulus, shear modulus and elastic constants. A standard molecular dynamics simulation code (MOLDY) [17] is used to calculate properties of Mg_3Bi_2 with a newly parametrized potential.

*corresponding author; e-mail: filizkayadibi@gmail.com

2. Computational technique and molecular dynamics simulation

2.1. Computational technique

In this study, we have developed semi-empirical potential parameters for the Born–Mayer–Huggins (BMH) form with Coulomb contribution that is given in Eq. (1):

$$\varphi_{ij}(r_{ij}) = \frac{Z_i Z_j e^2}{r_{ij}} + A \exp\left(-\frac{r_{ij}}{\rho}\right) - \frac{C}{r_{ij}^6}. \tag{1}$$

The first term is the Coulomb interaction between the effective charges Z_{ij}. Second term models the repulsion between the ions arising from the Pauli exclusion principle. Third term is the dipole–dipole contribution. r_{ij} is the distance between ions. Potential parameters are given in Table I.

TABLE I

The values of parameters in the potential given for Eq. (1) used for the MD simulations.

		A [eV]	ρ [A]	C [eV A^6]	Z
Bi	Bi	0.0	1.0	0.0	−2.04
Bi	Mg	1113.544811	0.38333	0.0	0.0
Mg	Mg	9547.96	0.21916	0.0	1.36

Parameters were adjusted to reproduce experimental data like lattice constants, bulk modulus and elastic constants where lattice constant is an experimental value [10, 18] and elastic properties are from first-principle calculations [15, 16]. Moreover, the Bredig

phase transition of Mg_3Bi_2 has been taken into account while obtaining potential parameters. Experimental measurements show that the $\alpha \rightarrow \beta$ transition takes place at 976 K [12] and melting at 1094 K, which is another critical point for the potential parameter development.

2.2. MD simulation

Molecular dynamics simulation of Mg_3Bi_2, consisting of 6655 particles with 3993 Mg^{2+} ions and 2662 Bi^{3-} ions, were performed at different temperatures up to 1600 K approximately 500 K above the experimental melting temperature. Mg_3Bi_2 has the hexagonal anti-La_2O_3 type structure (space group $P3m1$) with lattice parameters of 4.674 and 7.416, respectively [18]. $11 \times 11 \times 11$ simulation box with periodic boundary conditions is used to demonstrate the system. Simulations have been carried out by the molecular dynamics program, MOLDY [17]. We have used the Beeman algorithm, which integrates the Newton equation of motion, find positions and velocities of ions with the system time step $\Delta t = 1$ fs, here the total simulation time is 100 ps. When the system reached equilibrium after 30 ps, we average over the following 70 ps to calculate physical properties. The Ewald sum technique is used to obtain long-range Coulomb interactions. Our MD calculations have been performed in two parts. In the first part, initial configuration of the system is the crystal structure and the calculations are carried out from 300 K to 1600 K by restarting from the previous runs with 50 K intervals. In the second part, the system has been started as a liquid structure at 1100 K. Here the initial configuration is generated such that it is not periodic in three dimensions but with a regular minimum separation between center of masses. Molecules are placed at an interval that is called as skew start method. Second procedure is used in order to compare our radial distribution function with first-principle calculations where they also started their simulation with same initial configuration. All the calculations except the second procedure were performed in the constant pressure-temperature ensemble applying the Nosé–Hoover thermostat and the Parrinello and Rahman (P-R) constant stress method to control the temperature and pressure. Liquid structure simulations were performed in NVE ensemble for the density 5.467 g/cm^3.

3. Results and discussion

3.1. Radial distribution function

The radial distribution function, RDF, also called pair distribution function is one of the most important tools defining the structure of a system. The radial distribution function describes how the density changes as a function of distance from a reference particle, which is defined as following in Eq. (2):

$$g(r) = \frac{\Delta n(r)}{\rho 4\pi r^2 \Delta r}, \tag{2}$$

$\Delta n(r)$ is the mean number of atoms at a distance between r and $r + \Delta r$ from a given atom. ρ is the mean atom density and Δr is the width of the shell.

The radial distribution functions of Mg_3Bi_2 at 300 K and 1000 K are calculated. At 300 K, initial configuration is a crystal and for every 50 K interval restarted from the previous run up to 1000 K. For 1100 K, simulation is initiated from liquid configuration.

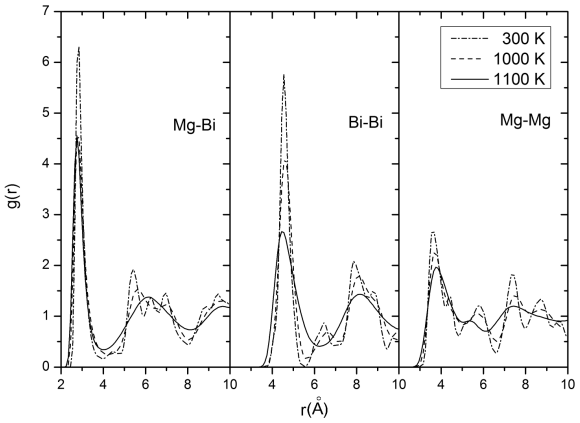

Fig. 1. The radial distribution functions of Mg_3Bi_2 at 300, 1000 and 1100 K.

In Fig. 1, the radial distribution functions of α-Mg_3Bi_2, β-Mg_3Bi_2 and liquid Mg_3Bi_2 are given from our MD calculations at 300, 1000, and 1100 K, respectively. As shown in the graph, all the peaks are narrow and sharp in the solid phase and as temperature increases to the liquid phase they gradually become shorter and wider because of the larger thermal oscillations of particles from their lattice points. At 1000 K, the $g_{\mathrm{MgMg}}(r)$ is rather broad and lower with less pronounced oscillations at larger r as compared to $g_{\mathrm{BiBi}}(r)$ which indicates that the cations are less structured than the anions with a higher Mg ion mobility like in the liquid phase so the $g_{\mathrm{BiBi}}(r)$ has a high degree of correlation as expected. This is a characteristic feature of a superionic (fast-ion) conductor [19] in which magnesium ions are the mobile ions with the bismuth ions forming the rigid lattice. Moreover we can also observe the first nearest neighbor separations between Mg–Mg, Bi–Bi, and Mg–Bi at 300 K and 1000 K from Fig. 1. First coordination peaks indicate the first nearest neighbor separations at 3.62, 4.54, and 2.84 Å at 300 K for Mg–Mg, Bi–Bi, and Mg–Bi, respectively, and it is also obtained from the same figure that values are 3.73, 4.59, and 2.80 Å at 1000 K, which agrees with the experimental values 3.75, 4.58, and 2.80 Å [11]. Additionally coordination number of Mg–Bi is calculated from Fig. 1 at 300 K with Eq. (3):

$$\left\langle n_{ij}(r)\,\Delta(r) = 4\pi r^2 \Delta r \rho_j g_{ij}(r) \right\rangle. \tag{3}$$

Number of j particles around i particles in a shell of Δr is given by $n_{ij}(r)\,\Delta r$. ρ_j is the number density of j particles in MD cell. We have calculated Bi–Mg coordination number where Bi atoms are surrounded by 7 Mg atoms and this result is in agreement with experimental data [20].

In Fig. 2, the radial distribution functions of liquid Mg_3Bi_2 at 1100 K are compared with the first principle

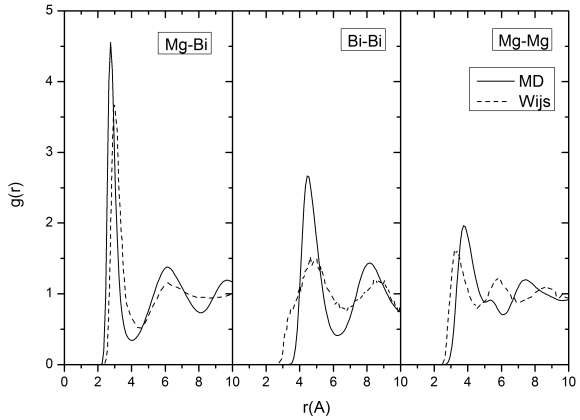

Fig. 2. The radial distribution functions of liquid Mg_3Bi_2 at 1100 K. Solid line represents our MD calculations and dashed line is the first principles calculations [9].

calculations [9] and these calculations are in good agreement with the Weber experimental data [21]. Both of the simulation results have the initial configuration of liquid structure where density is Mg_3Bi_2.

3.2. Lattice parameters, density and thermal expansion

We have obtained the lattice parameters of Mg_3Bi_2 with a constant pressure calculation, which is allowing the atoms in the unit cell relax to zero strain where it minimizes the total energy of the system. BFGS energy minimization strategy is used to search stationary point that is implanted in GULP program. $T = 0$ K lattice parameters are $a_0 = 4.61$, $c_0 = 7.2389$ and unit cell angles are $\theta_1 = 89.99$, $\theta_2 = 90.00$ and $\gamma = 119.99$. Cohesive energy per molecule is 4862.499 kJ/mol. Zhou et al. [15] have found the cohesive energy 2575.36 kJ/mol from first principle calculations. The calculated lattice parameters at room temperature are in fairly good agreement with available theoretical and experimental data [10, 15, 16, 18, 22–24]. All values of lattice parameters are given in Table II. We have also calculated the lattice parameters as a function of temperature. It has already been known that α-Mg_3Bi_2 does not melt directly but undergoes a transition to β phase at 976 K and β-phase melts at 1094 K [11]. The constant stress method of Parrinello and Rahman dynamics is used in the MD simulation. With this method, the system's shape can change and therefore both pressure and stress can be controlled. Eventually, lattice parameters in each dimension and each unit cell angles may change.

The variations of lattice constants a_1, a_2, c and the angles θ_1, θ_2, γ with temperature are shown in Figs. 3–5. The variation of density with temperature is given in Fig. 6. It is a well-known fact that MD overestimates the melting point of one phase crystal system. For this reason we have estimated the melting point about 1250–1300 K. This melting point will also be observed in other temperature dependent physical parameters through this article. Here in Figs. 3–5, structural

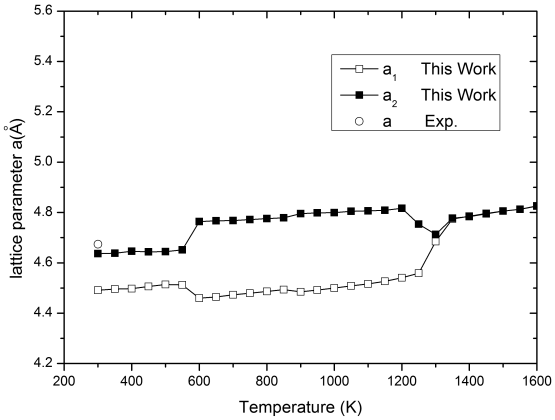

Fig. 3. Variation of lattice constant a with temperature.

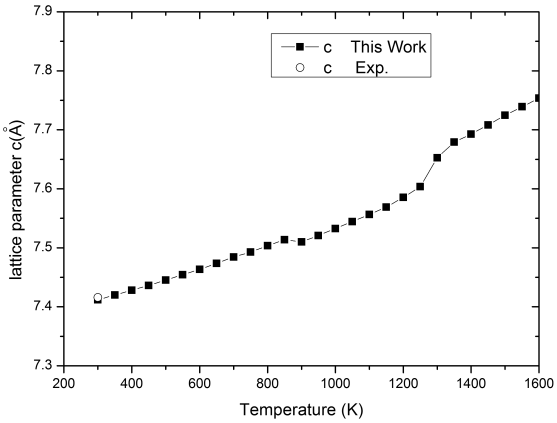

Fig. 4. Variation of lattice parameter c with temperature.

changes are monitored up to melting point. At around 500–600 K, lattice parameters a_1, a_2 for both directions change about 2%. At 850–900 K, lattice parameter a_1, a_2, c changes about 0.5%. Finally all three parameters change at MD melting point 1250 K–1300 K. These changes are also observed for angles θ_1, θ_2, γ in Fig. 5. These variations below the melting point may

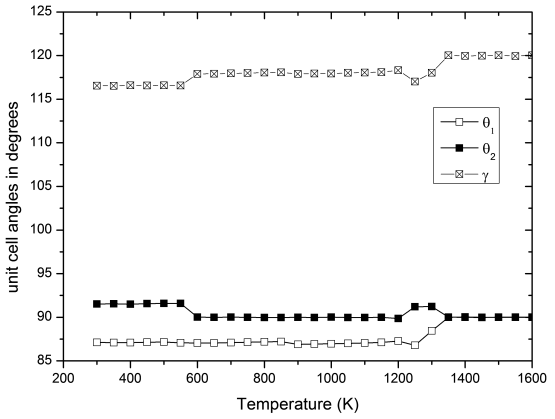

Fig. 5. Variation of unit cell angles with temperature.

TABLE II

Lattice constants (in Å) of α-Mg_3Bi_2.

Lattice constants			
	a	c	c/a
This work	4.61	7.24	1.571
[10]	4.666	7.401	1.586
[15]	4.67	7.41	1.586
[16]	4.66	7.333	1.573
[18]	4.674	7.416	1.586
[22]	4.671	7.403	1.584
[23]	4.67	7.40	1.584
[24]	4.65	7.38	1.587

be attributed to the $\alpha \rightarrow \beta$ phase transition. In Fig. 6, calculated density up to 1600 K compared with experimental data. At 300 K, density of Mg_3Bi_2 is in good agreement with experimental data. Again, it could also be observed that experimental melting point density of Mg_3Bi_2 (1100 K) and MD simulation melting point density of Mg_3Bi_2 (1250–1300 K) are also in good agreement. We can conclude that our MD simulation calculations with BMH potential display the structural distortions in phase transitions at correct temperatures.

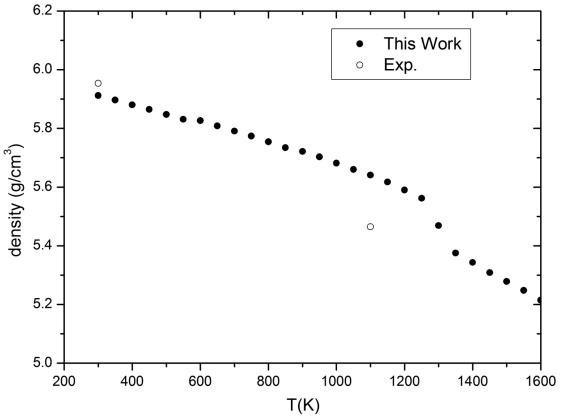

Fig. 6. Variation of density with temperature.

3.3. Diffusion of Mg^{2+} and Bi^{3-} sublattice

The mean square displacement (MSD) data of atoms in a simulation contains information on the atomic diffusivity. If the system is solid, the kinetic energy is not sufficient enough for atoms to reach a diffusive behavior, in such a case the slope of MSD is zero. Nevertheless if the system is not solid (e.g. liquid) then the MSD will change in time and the slope is different than zero where ions diffuse through the lattice. Mean square displacement of ionic species is a way to calculate the diffusion as follows:

$$\left\langle r_\alpha^2(t)\right\rangle = \frac{1}{3N_\alpha}\sum_{i\alpha}^{N\alpha}\left\langle \left|r_{i\alpha}(t) - r_{i\alpha}(0)\right|^2\right\rangle, \tag{4}$$

where $r_{i\alpha}(t)$ is the position of the i-th ion at time t. The mean square displacements of Mg^{2+} and Bi^{3-} ions from the room temperature up to 1300 K for $11\times11\times11$ supercell are presented in Fig. 7 as a function of time. It has been reported that α-Mg_3Bi_2 in solid state has a second order structural transition to the superionic phase at nearly 976 K [11]. Superionic phase transition can be explained as: an order-disorder transition starts by the collapse of Mg^{2+} sub-lattice and Mg^{2+} ions behave like a liquid while Bi^{3-} ions are still solid. In such a case the behaviors of ions correspond to the superionic phase transition. Diffusion for Mg^{2+} ions are almost zero up to 1000 K. Above this point Mg diffusion starts and Bi also shows signs of mobility that we do not expect at this temperature. This could be commented that melting and superionic phase transition temperatures are relatively too close to each other about 100 K for a MD simulation. Otherwise, if there would be a larger gap between transition and melting point temperature, we should observe Bi ions totally immobile, preserving its rigid sublattice at the superionic transition temperature. It is a generally known issue that MD simulations overestimate the melting temperature [25]. Even there exist no general rules that we would deduce from the previous studies that melting temperature of solid MD box is about 20%–30% above the experimental data [26]. In this study, melting point of the Mg_3Bi_2 molecule is also overestimated. At 1300 K, in Fig. 7, we could clearly observe both sublattices totally collapsed. From this we could deduce that melting temperature is about 1250–1300 K where the experimental value is 1094 K.

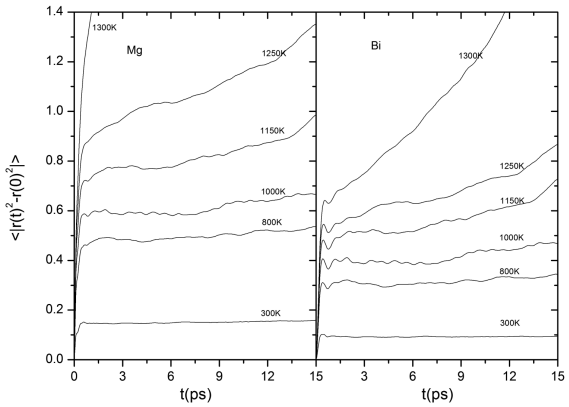

Fig. 7. Mean square displacements of Mg^{+2} and Bi^{-3} ions.

The diffusion constant of ions using the Einstein relation can be calculated from the gradient of the MSD graph

$$\left\langle \left|r_{i\alpha}(t) - r_{i\alpha}(0)\right|^2\right\rangle = 6Dt \tag{5}$$

or diffusion coefficient may also be calculated from the velocity auto-correlation function (VACF). Following relation shows VACF function

$$C(t) = \langle \boldsymbol{V}_i(t_0)\cdot\boldsymbol{V}_i(t_0+\tau)\rangle = \frac{1}{N}\sum_{i=1}^{N}\frac{1}{t_{\max}}\sum_{t_0=1}^{t_{\max}}\boldsymbol{V}_i(t_0)\cdot\boldsymbol{V}_i(t_0+\tau), \tag{6}$$

where N is the particle number. Diffusion coefficient (D) is

$$D = \frac{1}{3}\int_0^\infty C(t)\,\mathrm{d}t. \tag{7}$$

Diffusion coefficients of Mg_3Bi_2 molecules are shown in Fig. 8, which are calculated from VACF and MSD data, and display slightly different behavior up to 650 K. In spite of discrepancies at low temperatures, it should be noted that this is a logarithmic plot and the values are too small when it is compared with high temperatures. Both of the calculations of diffusion coefficient increase with temperature and at about 1050 K Mg diffusion coefficient changes anomalously when compared to Bi. Diffusion coefficient of Mg ion is higher than Bi ion above the $\alpha \rightarrow \beta$ phase transition temperature.

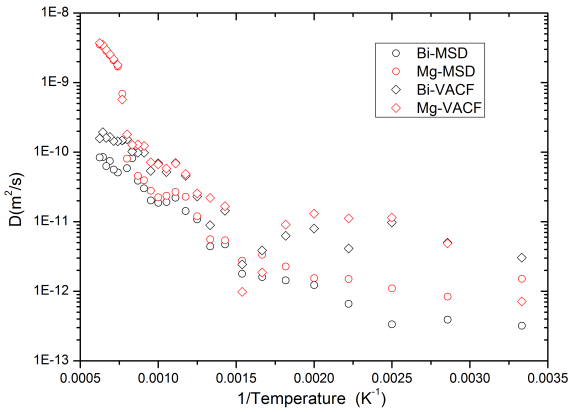

Fig. 8. An Arrhenius plot of Mg_3Bi_2 from 300 K up to 1600 K.

In literature there is a limited number of experimental data on diffusion of Mg_3Bi_2 as far as we know. Howells [12] had measured the diffusion coefficient of Mg ions by neutron scattering experiment. He concluded that the diffusion coefficient is $2.7\pm0.3\times10^{-9}$ m^2/s for both β and liquid phases. From Fig. 8, our estimated value of Mg ion diffusion coefficient for the liquid phase (2.18×10^{-9} m^2/s is in agreement with experimental data.

3.4. Enthalpy and heat capacity

α-Mg_3Bi_2 molecule has a phase transitions from $\alpha \rightarrow \beta$ and $\beta \rightarrow$ melting point. For these reason it is a good idea to investigate energy and related properties. Enthalpy curve is a useful tool to observe phase transitions. The enthalpy change $\Delta H = H_T - H_{300}$ is presented in Fig. 9. A discontinuity of data indicates some abnormal phenomena are taking place like the phase transition. In Fig. 10, the specific heat at constant pressure can be determined from the variation of the internal energy of the system with temperature as

$$C_P(T) = \left(\frac{\partial E}{\partial T}\right)_P. \tag{8}$$

In Fig. 10, estimated value of heat capacity is equal to classical value of the Dulong–Petit law. As the temperature increases, the slope of heat capacity changes gently by the creation of magnesium Frenkel pairs. When we compare Mg and Bi ions from the diffusion data, Mg ions are inherently more mobile. As a result of these, it can be stated that much of the Frenkel pairs are Mg. Between 800–1100 K, small deviations from the classical heat capacity value can be attributed to the change of lattice parameters a and c. From 1100 K to 1400 K there exists a rapid increase in the heat capacity data. Here, both superionic transition and melting point appear in this temperature range. One can deduce this from MSD in Fig. 7 and in general every phase change indicates itself in energy data. Here the phase transitions, $\alpha \rightarrow \beta$ (976 K) and $\beta \rightarrow$ melting point (1094 K), are so close that it can be concluded that these peaks merged into one peak.

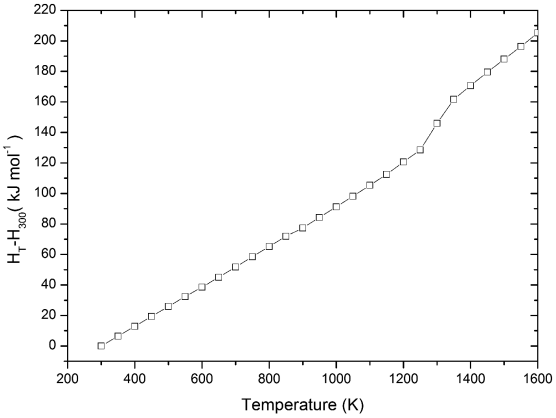

Fig. 9. Enthalpy change of Mg_3Bi_2 with temperature.

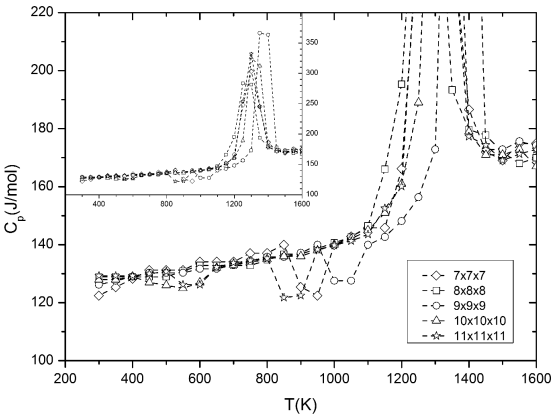

Fig. 10. Heat capacity of Mg_3Bi_2 for different supercell sizes change with temperature.

3.5. Elastic constants, bulk modulus and shear modulus

Hardness of a material is determined with the elastic constants, bulk and shear modules. These constants are calculated by different types of deformations of the crystal. Bulk modulus can be measured by the Birch–Murnaghan equation of state. When isotropic pressure

is applied to a material, this equation is fitted to the variation of energy or variation of pressure with the volume

$$B = V\left(\frac{\partial^2 U}{\partial V^2}\right) = -V\left(\frac{\partial P}{\partial V}\right). \quad (9)$$

U is the energy, V is the volume and P is the pressure. Equation of state data can be easily obtained from the MD simulation by changing the volume around the minimum energy point. Bulk and shear modules can also be calculated by the combination of elastic constants

$$B = \frac{1}{9}\left(C_{11} + C_{22} + C_{33} + 2\left(C_{12} + C_{13} + C_{23}\right)\right), \quad (10)$$

$$G = \frac{1}{15}\left(C_{11} + C_{22} + C_{33} + 3\left(C_{44} + C_{55} + C_{66}\right) - C_{12} - C_{13} - C_{23}\right). \quad (11)$$

These equations are Voigt definition of bulk and shear modulus. Shear modulus describes the crystal's response to shear stress. Elastic properties are estimated from the second-order derivatives of the potential with respect to strain

$$C_{ij} = \frac{1}{V}\left(\frac{\partial^2 U}{\partial \varepsilon_i \partial \varepsilon_j}\right). \quad (12)$$

Here ε is the deformation. Since α-Mg_3Bi_2 is a non-cubic material, C_{13}, C_{33} should also be investigated in addition to C_{11}, C_{12} and C_{44}. All the elastic properties are investigated by GULP program [27]. To the best of our knowledge there are only two measured values of α-Mg_3Bi_2 bulk modulus [15, 16]. Both of them are first-principle calculations and different from each other by about 15%. Shear and elastic modulus data are only compared with one calculated data [15]. Most of our results, except C_33 and C_44, are in good agreement with quantum chemical calculation that is given in Table III.

TABLE III

Elastic properties of Mg_3Bi_2.

	Ab initio	Present work
bulk modulus [GPa]	45.81 [15]/ 39.8 [16]	39.03
shear modulus [GPa]	7.96 [15]	7.92
C_{11} [GPa]	64.26 [15]	69.77
C_{33} [GPa]	103.64 [15]	41.55
C_{12} [GPa]	36.59 [15]	47.67
C_{13} [GPa]	39.53 [15]	25.15
C_{44} [GPa]	4.04 [15]	22.59

4. Conclusions

In this study, we have investigated Mg_3Bi_2 from room temperature to 1600 K by molecular dynamics simulation with newly developed potential parameters of BMH type potential. Lattice parameters, elastic constants, bulk modulus and shear modulus are the main observables and reference data while we are developing the potential parameters. As we increase the temperature, phase transitions, $\alpha \rightarrow \beta$ and $\beta \rightarrow$ melting point, are also taken into account.

Lattice parameters are calculated as $a = 4.61$ Å and $c = 7.24$ Å and compared with a considerable amount of experimental and first principle data [10, 15, 16, 18, 22–24] which are in agreement with these results (Table II). As the temperature increases from room temperature to 1600 K, constant stress method of Parrinello and Rahman dynamics is used where lattice parameters change in each dimension so that lattice constant a_1 and a_2 diverge from each other and angles do not maintain their $\alpha = 90°$, $\beta = 90°, \gamma = 120°$ values. Among the NPT ensembles constant stress method of P-R is chosen in order to avoid uniform dilation or contraction of Mg_3Bi_2 crystal structure where it is experimentally known that as the temperature increases hexagonal Mg_3Bi_2 structure changes into β-Mg_3Bi_2 structure by the non-uniform change of lattice parameters and angles. Experimental density at room temperature is 5.95 g/cm^3 and 5.465 g/cm^3 at melting point. Our results are 5.91 g/cm^3 and 5.468 g/cm^3, respectively. Room temperature and liquid phase densities are in agreement with experimental data but it should be noted that MD melting point temperature is overestimated about 200 K which is normal for one phase supercell simulation box system. Radial distribution functions of liquid Mg_3Bi_2 are also compared with first-principle calculations. Except Bi–Bi first peak, they roughly have the same behavior.

RDF peak positions are in good agreement with experimental values for both room temperature and melting point data. Howells commented on his empirical diffusion coefficient value of Mg ion which it is the same both for the superionic phase and liquid phase whereas we think this should be reconsidered again because temperature difference between these two points are 100 K and diffusion constant could not be the same. Nevertheless, liquid diffusion coefficient derived both from mean square displacement and velocity auto-correlation functions for liquid phase confirm that our results are compatible with the experimental value. Sedighi [16] and Zhou [15] calculated the bulk modulus from first principle with a certain amount of value (15%) different from each other, which makes these values somewhat unreliable and these data needs to be verified by experimental methods. Our data significantly resembles the latest first principle calculation by Sedighi [16]. Zhou et al. also obtain values of elastic properties, like elastic constants, shear modulus. Our calculated values are in agreement with shear modulus, C_{11}, C_{12} and C_{13}. All these results display the features of promising classical interaction potential parameters for MD simulation of Mg_3Bi_2 which is valid for a broad temperature range.

References

[1] B.L. Mordike, T. Ebert, *Mater. Sci. Eng. A* **302**, 37 (2001).

[2] A. Luo, M.O. Pekgüleryüz, *J. Mater. Sci.* **29**, 5259 (1994).

[3] H. Honda, H. Sakaguchi, I. Tanaka, T. Esaka, *J. Power Sources* **123**, 216 (2003).

[4] T. Kajikawa, N. Kimura, T. Yokoyama, *Thermoelectrics* **ICT 2003**, 305 (2003).

[5] P. Singh, K.K. Sarkar, *Solid State Commun.* **55**, 439 (1985).

[6] L.W. Watson, C.A.W. Marshall, C.P. Cardoso, *J. Phys. F Met. Phys.* **14**, 113 (1984).

[7] G. Yuan, Y. Sun, W. Ding, *Mater. Sci. Eng. A* **308**, 38 (2001).

[8] G. Yuan, M. Liu, W. Ding, I. Akihisa, *Mater. Sci. Eng. A* **357**, 314 (2003).

[9] G.A. de Wijs, G. Pastore, A. Selloni, W. van der Lugt, *J. Phys. Condens. Matter* **8**, 1879 (1996).

[10] *Crystal Structures*, Ed. R.W.G. Wyckoff, 2nd ed., Vol. 1, Wiley, New York 1963.

[11] A.C. Barnes, C. Guo, W.S. Howells, *J. Phys. Condens. Matter* **6**, L467 (1994).

[12] W.S. Howells, A.C. Barnes, M. Hamilton, *Physica B* **266**, 97 (1999).

[13] C. Guo, A.C. Barnes, W.S. Howells, *J. Phys. Condens. Matter* **8**, 10823 (1996).

[14] Q.H. Hao, Y.W. You, X.S. Kong, C.S. Liu, *Int. J. Mod. Phys. B* **27**, 1350011 (2013).

[15] D.W. Zhou, J.S. Liu, S.H. Xu, P. Peng, *Physica B* **405**, 2863 (2010).

[16] M. Sedighi, B.A. Nia, H. Zarringhalam, R. Moradian, *Eur. Phys. J. Appl. Phys.* **61**, 10103 (2013).

[17] K. Refson, *Comput. Phys. Commun.* **126**, 310 (2000).

[18] *Structure and Properties of Inorganic Solids*, Ed. F.S. Galasso, Pergamon Press, Oxford 1970, p. 157.

[19] *Physics of Superionic Conductors*, Ed. M.B. Salamon, Springer, Berlin 1979.

[20] *Structural Inorganic Chemistry*, Ed. A.F. Wells, 4th ed., Clarendon Press, Oxford 1975.

[21] M. Weber, S. Steeb, P. Lamparter, *Z. Nat.forsch. A* **34**, 1398 (1979).

[22] E. Zintl, E. Husemann, *Z. Phys. Chem. B* **21**, 138 (1933).

[23] Y. Imai, A. Watanabe, *J. Mater. Sci.* **41**, 2435 (2006).

[24] L.G. Sevast'yanova, O.V. Kravchenko, O.K. Gulish, V.A. Stupnikov, M.E. Leonova, M.G. Zhizhin, *Inorg. Mater.* **42**, 863 (2006).

[25] F. Ercolessi, S. Iarlori, O. Tomagnini, E. Tosatti, X.J. Chen, *Surf. Sci.* **251/252**, 645 (1991).

[26] J.R. Morris, C.Z. Wang, K.M. Ho, C.T. Chan, *Phys. Rev. B* **49**, 3109 (1994).

[27] J.D. Gale, A.L. Rohl, *Mol. Simul.* **29**, 291 (2003).